

**SAGACE:**  
**the Spectroscopic Active Galaxies And Clusters Explorer**

P. DE BERNARDIS<sup>1\*</sup>, D. BAGLIANI<sup>2</sup>, A. BARDI<sup>3</sup>, E. BATTISTELLI<sup>1</sup>, M. BIRKINSHAW<sup>4</sup>,  
M. CALVO<sup>1</sup>, S. COLAFRANCESCO<sup>5</sup>, A. CONTE<sup>1</sup>, S. DE GREGORI<sup>1</sup>, M. DE PETRIS<sup>1</sup>, G.  
DE ZOTTI<sup>6</sup>, A. DONATI<sup>3</sup>, L. FERRARI<sup>2</sup>, A. FRANCESCHINI<sup>6</sup>, F. GATTI<sup>2</sup>, M. GERVASI<sup>7</sup>,  
P. GIOMMI<sup>5</sup>, C. GIORDANO<sup>1</sup>, J. GONZALEZ-NUEVO<sup>8</sup>, L. LAMAGNA<sup>1</sup>, A. LAPI<sup>9</sup>, G.  
LUZZI<sup>1</sup>, R. MAIOLINO<sup>10</sup>, P. MARCHEGIANI<sup>5</sup>, A. MARIANI<sup>3</sup>, S. MASI<sup>1</sup>, M. MASSARDI<sup>8</sup>,  
P. MAUSKOPF<sup>11</sup>, F. NATI<sup>1</sup>, L. NATI<sup>1</sup>, P. NATOLI<sup>9</sup>, M. NEGRELLO<sup>12</sup>, F. PIACENTINI<sup>1</sup>, G.  
POLENTA<sup>1</sup>, M. SALATINO<sup>1</sup>, G. SAVINI<sup>13</sup>, A. SCHILLACI<sup>1</sup>, S. SPINELLI<sup>7</sup>, A. TARTARI<sup>7</sup>,  
M. TAVANTI<sup>3</sup>, A. TORTORA<sup>3</sup>, M. VACCARI<sup>6</sup>, R. VACCARONE<sup>2</sup>, M. ZANNONI<sup>7</sup>, V.  
ZOLESI<sup>3</sup>

<sup>1</sup>*Dipartimento di Fisica, Università La Sapienza, and INFN sezione di Roma, Roma, Italy;*

<sup>2</sup>*Dipartimento di Fisica, Università di Genova, and INFN sezione di Genova, Italy;* <sup>3</sup>*Kayser Italia, Livorno, Italy;* <sup>4</sup>*Department of Physics, University of Bristol, UK;* <sup>5</sup>*ASDC - ASI - Frascati, Italy;* <sup>6</sup>*INAF, Osservatorio di Padova, Italy;* <sup>7</sup>*Dipartimento di Fisica, Università di Milano Bicocca, Italy;* <sup>8</sup>*SISSA - Trieste, Italy;* <sup>9</sup>*Dipartimento di Fisica, Università di Tor Vergata, Roma, Italy;* <sup>10</sup>*INAF - Osservatorio di Roma, Italy;* <sup>11</sup>*Department of Physics and Astronomy, Cardiff University, UK;* <sup>12</sup>*Department of Physics and Astronomy, Open University, Milton Keynes, UK;* <sup>13</sup>*Department of Physics and Astronomy, University College London, UK;*  
\* e-mail: paolo.debernardis@roma1.infn.it

The SAGACE experiment consists of a mm/sub-mm telescope with a 3-m diameter primary mirror, coupled to a cryogenic multi-beam differential spectrometer. SAGACE explores the sky in the 100-760 GHz frequency range, using four diffraction-limited bolometer arrays. The instrument is designed to perform spectroscopic surveys of the Sunyaev-Zeldovich effects of thousands of galaxy clusters, of the spectral energy distribution of active galactic nuclei, and of the [CII] line of a thousand galaxies in the redshift desert. In 2008 a full phase-A study for a national small mission was completed and delivered to the Italian Space Agency (ASI). We have shown that taking advantage of the differential operation of the Fourier Transform Spectrometer, this ambitious instrument can operate from a Molniya orbit, and can be built and operated within the tight budget of a small mission.

*Keywords:* Cosmology, Clusters of Galaxies, Early Galaxies, Cosmic Microwave Background, Space Experiments, Spectrometers

## 1. SAGACE Science

Our knowledge of the mm/sub-mm sky is rapidly improving. Balloon-borne missions and the recent WMAP all-sky survey have produced impressive maps of the cosmic microwave background (CMB), allowing the precise measurement of several cosmological parameters. The Planck<sup>1,2</sup> mission is producing maps of the whole sky in nine wavebands with exquisite accuracy, allowing a secure separation of the CMB signals from the Galactic and extragalactic foregrounds, and a massive shallow survey of Sunyaev-Zeldovich clusters.

However, the spectroscopic exploration of the frequency range between 90 and 600 GHz is still completely undeveloped, since most of this range is not accessible

from the ground. In the past, the FIRAS survey on COBE<sup>3</sup> has produced coarse ( $10^\circ$ ) spectral maps of the sky with an absolute Fourier Transform Spectrometer (FTS). The main components in the measured spectra are the CMB, the continuum emission of diffuse interstellar dust, and a few prominent lines from the interstellar medium ([CII], [OIII], ...). We simply do not have higher-resolution surveys with significant sky coverage, and the currently-operating Herschel spectroscopic instrument (SPIRE) will cover only frequencies higher than 450 GHz<sup>4</sup> with a small field of view.

Diffuse emission in the mm/sub-mm range is very rich in astrophysical and cosmological information. This motivated our proposal for a 3-m space telescope coupled to a Fourier Transform Spectrometer, covering the range 100-760 GHz with four arrays of diffraction-limited, photon-noise-limited cryogenic bolometers. In the following we describe a few of the many topics accessible with a high sensitivity spectroscopic survey of diffuse emission at these frequencies. Then, we will outline our baseline proposal for a small (cost-wise) mission, with ambitious goals.

### 1.1. *Sunyaev-Zeldovich effect*

A fundamental topic of current cosmological research is the study of the formation and evolution of cosmic structures. Clusters of galaxies represent an extremely important structural level in this framework. They are the largest gravitationally-bound structures in the Universe, and can contain up to a few thousand galaxies. The cluster volume between galaxies is filled with a hot ( $10^7$ - $10^8$  K), ionized gas which makes up a significant fraction ( $\sim 10$ - $20$  %) of the total mass of the cluster. In addition, the presence of a dominant dark mass component is required to explain the motions of galaxies in clusters and the gravitational lensing of background galaxies.

The presence of ionized gas in the intracluster medium is evident from X-ray observations of clusters of galaxies. Here clusters appear as diffuse sources, with the ionised gas filling the potential well of dark matter, heated to millions of degrees, and producing intense thermal bremsstrahlung emission. The same particles of the ionized intracluster gas interact with the CMB via the inverse-Compton effect, the up-scattering of low-energy photons off more energetic hot electrons. This phenomenon, also known as the Sunyaev-Zeldovich Effect (SZE), produces an additional source of anisotropy in the CMB in the direction of rich clusters of galaxies.

The optical depth for this effect is small, but not negligible, because although the density of electrons is only of order  $n_e \sim 10^{-3} \text{ cm}^{-3}$ , the path length  $\ell$  through a cluster medium can be several Mpc. With a Thomson cross section  $\sigma = 6.65 \times 10^{-25} \text{ cm}^2$ , this produces an optical depth  $\tau = n_e \sigma \ell \sim 0.01$ . So we have a 1% probability that a CMB photon crossing a rich cluster is scattered by an electron. Since the electron energy is much larger than the energy of the photon, to first order the fractional energy gain for the photon is about  $kT_e/m_e c^2 = 1\%$ . The resulting fractional temperature change of the CMB is of the order of  $1\% \times 1\% = 10^{-4}$ ,

corresponding to an anisotropy of about  $300 \mu\text{K}$  in the direction of the cluster. This is a large signal relative to the tens of  $\mu\text{K}$  level of the CMB anisotropy, and the few  $\mu\text{K}$  component of this at arcmin angular scales. This is the thermal part of the SZE.

Being a scattering effect, the SZE does not depend on the distance of the cluster. For high-redshift clusters, the decrease in solid angle with increasing redshift is exactly compensated by the increase of the local temperature of the CMB. Therefore distant clusters of galaxies that are too faint to be detected in the X-ray or optical bands can still be observable via the SZE.

The spectrum of the thermal SZE has a characteristic shape. Since all interacting CMB photons get approximately a 1% boost in energy, the result is a transfer of photons in the CMB spectrum from lower to higher frequencies, resulting in a decrease of brightness at low frequencies (below 217 GHz) and an increase of brightness at high frequencies (above 217 GHz), as shown in Fig. 1.

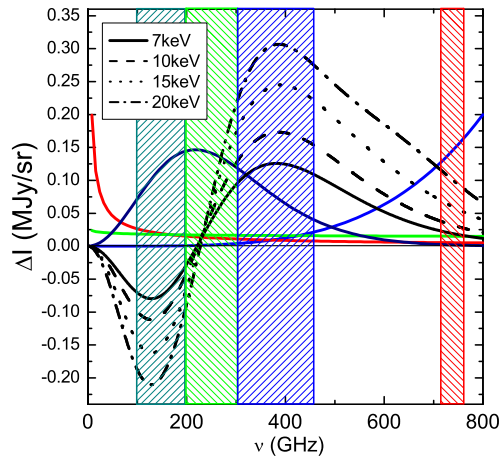


Fig. 1. Spectrum of the thermal SZE in clusters of galaxies. Plotted (black lines) is the difference between the CMB spectrum through the cluster and the CMB spectrum outside the cluster. The different black lines refer to different temperatures of the intracluster plasma. The other lines represent the spectral shapes (not normalized) of different contaminants: synchrotron (red), free-free (green), CMB anisotropy and kinetic SZE (dark blue), dust (blue). This shows that the thermal SZE spectrum can easily be distinguished from contaminants by measurements over sufficient spectral range. The shaded areas represent the four observation sub-bands of the SAGACE instrument.

Thus the same cluster will be seen as a dark spot in the CMB at frequencies below 217 GHz, and as a bright spot at frequencies above 217 GHz. This unusual spectrum makes it possible to extract the SZE signal even in the presence of contaminating sources, like confusion from the CMB anisotropy itself, Galactic emission,

and unresolved extragalactic sources.

In addition to the thermal signal, other sources of SZE can be produced in clusters via the interaction of non-thermal (relativistic and sub-relativistic) particle distributions with the CMB photons, providing SZE signals with specific spectral and spatial characteristics.<sup>6</sup>

The key strategy to perform the SZE signal extraction is to have spectral coverage of both the negative and positive sides of the SZE.

A spectroscopic mission like SAGACE is optimized to extract the SZE from all the other diffuse components, even in distant and low-mass clusters. Operating from space, SAGACE will not be affected by atmospheric absorption and noise, the main limiting factors for current wide-field deep surveys of SZE clusters. The number of independent bands observable from the ground is limited in number and spectral range. This results in bias and degeneracies between the different cluster parameters recovered from SZE measurements (mainly the optical depth, the peculiar velocity, the temperature of the gas). All these problems are solved by a wide coverage spectrometer (see Sec. 4). Furthermore, the coverage of the whole interesting spectral range with a single instrument will solve the major problem of the cross-calibration of different instruments affecting current measurements.

### 1.2. *Star forming galaxies at the peak of cosmic activity*

The density of cosmic star formation rate peaks at  $z \sim 1.5$ . This is the epoch where galaxies form and assemble at the highest rate, either through merging or through enhanced gas accretion. Paradoxically, the redshift interval  $1.2 < z < 2$  is the most difficult to investigate spectroscopically from the ground. Indeed, while optical spectrographs with high multiplexing have been effective in identifying the redshift of large samples of galaxies at  $z < 1.2$  and at  $z > 2$ , at intermediate redshifts (the so called “redshift desert”) the most prominent emission features (e.g. Ly- $\alpha$ , [OII],...) used to spectroscopically identify galaxies are outside the optical band. This has hampered studies of galaxies in the most important redshift range. Currently, less than 10% of star forming galaxies have been spectroscopically identified within the redshift desert.<sup>7</sup>

The far-IR spectral band hosts the brightest lines in the spectrum of any galaxy (Fig. 2). In particular the [CII] line at  $158 \mu\text{m}$  is generally the strongest line in the spectrum of nearly all galaxies, accounting for as much as 1% of the galaxy bolometric luminosity. The use of this and other far-IR lines is currently limited to the local Universe (through space missions such as ISO and Herschel<sup>8</sup>) and to a few very high redshift targets ( $z > 4$ ) for which such far-IR lines are redshifted into the (sub)mm atmospheric windows<sup>9-11</sup>. The lack of space observatories with sensitive spectroscopic capabilities in 700-800 GHz has prevented astronomers from exploiting these emission lines to identify galaxies around the epoch of peak cosmic star formation.

The high resolution spectroscopic mode of SAGACE at high frequencies (720-760

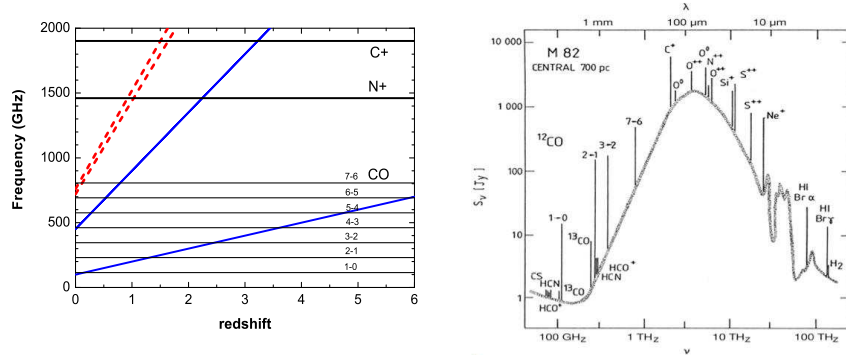


Fig. 2. Left: Redshift dependence of the frequency coverage of SAGACE, compared to the rest-frame frequencies of important lines from the diffuse medium in galaxies. The bands explored by SAGACE lie between the two solid (blue) lines and between the two dashed (red) lines. Right: Spectrum of M82, showing the continuum and the lines used in the left panel. The 158- $\mu\text{m}$   $\text{C}^+$  line is the brightest cooling line in galaxies.

GHz) will allow us to identify the redshift of large samples of star forming galaxies at  $1.5 < z < 1.6$ , well within the redshift desert, by detecting their [CII] line (Fig. 2). In particular the fast mapping speed of SAGACE at this frequency will allow the detection of several thousands of galaxies in this redshift range. The [CII] line will not only provide the redshifts of the sources but also an indication of their star formation rate (since [CII] is the main coolant of the ISM). By detecting thousands of galaxies it will also be possible to determine the three-dimensional clustering of galaxies at  $z \sim 1.5$ , which will allow us to trace the evolution of cosmic structures around this crucial epoch with unprecedented detail, with important cosmological implications.

### 1.3. Active Galactic Nuclei

SAGACE will also perform a wide area ( $> 1000 \text{ deg}^2$ ) deep photometric survey down to the confusion limit, thus providing a unique database for investigating the cosmological evolution of the luminosity function and of the spectral energy distribution of Active Galactic Nuclei (AGN) and of star-forming galaxies over a broad redshift interval, in the poorly explored but crucial microwave-to-submillimeter wavelength range (see Fig. 3).

## 2. The SAGACE Instrument

SAGACE has been proposed as a small mission, answering a recent call of the Italian Space Agency. The design is the result of a trade-off between scientific ambitions and severe limitations of weight, complexity and cost.

SAGACE is mainly a mm/sub-mm spectroscopic mission, taking advantage of the high broad-band sensitivity of cryogenic bolometric detectors. To achieve a wide

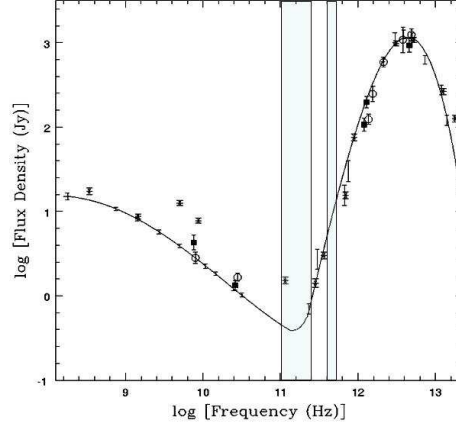


Fig. 3. The continuous line represents the best fit spectral energy distribution (SED) of the prototypical starburst galaxy (M82).<sup>5</sup> The different symbols indicate the measurements for several quasars and luminous infrared galaxies, normalized to fit the peak emission of M82. The spectral coverage of SAGACE is represented by the two shaded areas, and includes the transition from synchrotron-dominated to dust-dominated emission.

spectral range (100-760 GHz) with imaging capabilities and components with proven readiness for space use, a Fourier Transform Spectrometer (FTS) has been selected. In particular, we are considering as the baseline a Martin-Puplett architecture,<sup>12</sup> because it allows a clean differentiation of the spectra coming from two independent inputs. In our case the two inputs cover two contiguous areas of the focal plane, so that the measured spectrum is the difference between the spectrum of the target source and the spectrum of an offset reference field. This is sketched in Fig. 4.

With this differential configuration, very small signals (like the SZE distortion of the CMB in the direction of a cluster) can be extracted from an overwhelming common mode background, generated by the CMB itself, plus the emission of the warm telescope (radiatively cooled to about 80 K), plus most of the spillover from the Earth. The FTS has the important advantage over dispersion spectrometers of being an imaging instrument. 2D detector arrays can be accommodated in the focal plane, boosting the mapping speed.

At these wavelengths, the achievable angular resolution is limited by diffraction at the entrance aperture of the telescope. The largest size of a primary mirror which can fit the Soyuz bay is about 3.0 m; the rest of the available diameter is occupied by the shields necessary to limit the sidelobes of the telescope, a critical issue at these wavelengths. Budget constraints do not allow us to consider deployable mirror solutions. We have included in our baseline design a large (12 m diameter) deployable Earth shield.

In order to limit the radiative background (and the corresponding fluctuations) on the detectors, and to match the detector size to the diffraction-limited angular resolution (which improves with increasing frequency), we have divided our spectral

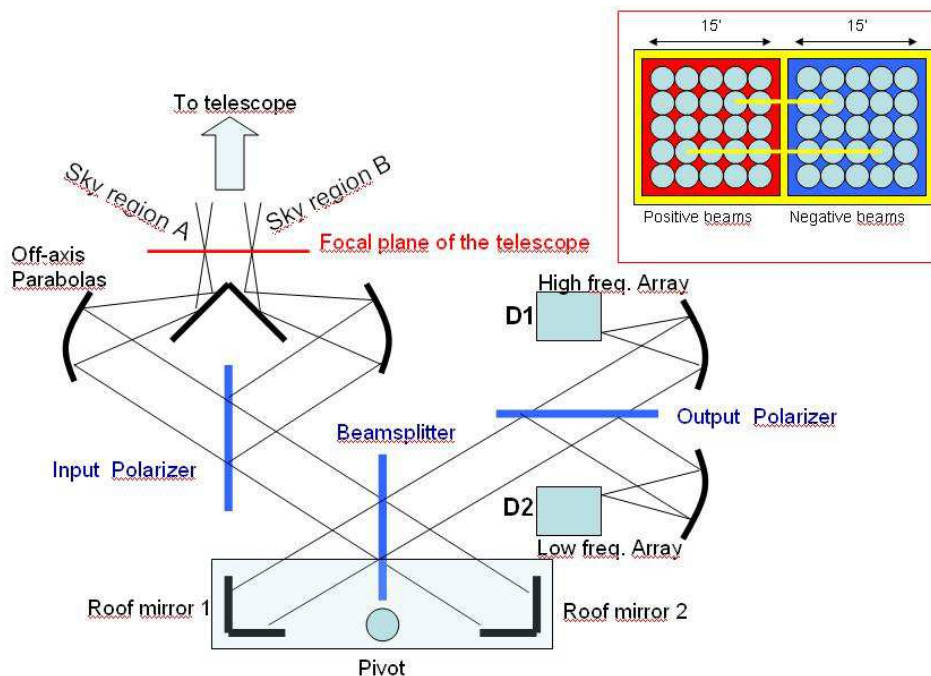


Fig. 4. Conceptual diagram of the SAGACE spectrometer and of its focal plane configuration. The two inputs of a Martin-Puplett polarizing interferometer are located in two contiguous sections of the focal plane of the SAGACE telescope. This enables angular differentiation of the sky brightness, as detailed in the top-right inset

range into four bands. These bands have been optimized for performance in the study of the SZE, taking into account the background emission from the warm telescope and from the interstellar medium in our Galaxy.

The bands resulting from this optimization are  $B_1 = 100 - 200$  GHz,  $B_2 = 200 - 300$  GHz,  $B_3 = 300 - 450$  GHz, and  $B_4 = 720 - 760$  GHz. With a 3-m diameter dish the corresponding angular resolutions are 4.5, 2.25, 1.5, and 0.75 arcmin FWHM, respectively. A  $15' \times 15'$  field of view (resulting in two contiguous FOVs in the sky, see Fig. 4) is filled with diffraction limited detectors: the resulting number of detectors per band is 9, 36, 81, and 324. The photon background is dominated by the warm telescope (at  $\sim 80$  K), and is of order 0.8, 0.3, 0.2, and 0.1 pW in the four bands. The achievable photon-noise limited NEP of each of the detectors is thus  $(1.3, 1.0, 1.2, \text{ and } 0.8) \times 10^{-17} \text{ W}/\sqrt{\text{Hz}}$ .

The spectral resolution of the instrument depends on the maximum delay introduced between the two beams of the interferometer. We have selected a double pendulum configuration,<sup>13</sup> which has been used several times in space missions, due to its simplicity and reliability of the movement. This is very important in a cryogenic implementation as ours. Our moving mirrors are moved by tilting their supporting frame around a flexural pivot, completely avoiding bearings. Resonance

oscillation of the frame requires little energy for motion control, thus maximising cryogen lifetime. A double interferometer configuration, similar in spirit to the one described in<sup>14</sup> has been designed, so that all the power coming from the sky is processed by the instrument. The maximum optical path difference (OPD) introduced by the motion of the mirrors is 180 mm, resulting in 1-GHz resolution over the full 100-760 GHz frequency range. A low-resolution mode with 9 mm OPD and 20 GHz resolution is also available.

The detectors are fed by a fast Ritchey-Chrétien telescope, with a 3-m diameter primary mirror. The entrance pupil is limited to 2.8 m in diameter by a cold Lyot stop. The secondary mirror diameter is 45 cm, and the equivalent focal length of the telescope is 9.2 m, while the distance between the subreflector and the focal plane is only 1.47 m. The telescope is surrounded by a fixed inner shield, and by a large (12 m diameter) deployable Sun/Earth shield. The survey strategy is optimized to keep the Sun, the Moon and the Earth at more than  $90^\circ$  from the telescope axis during observations. In this way, stray radiation from these sources has to undergo two diffractions before hitting the edge of the primary mirror. An artist's impression of the SAGACE satellite is shown in Fig. 5.

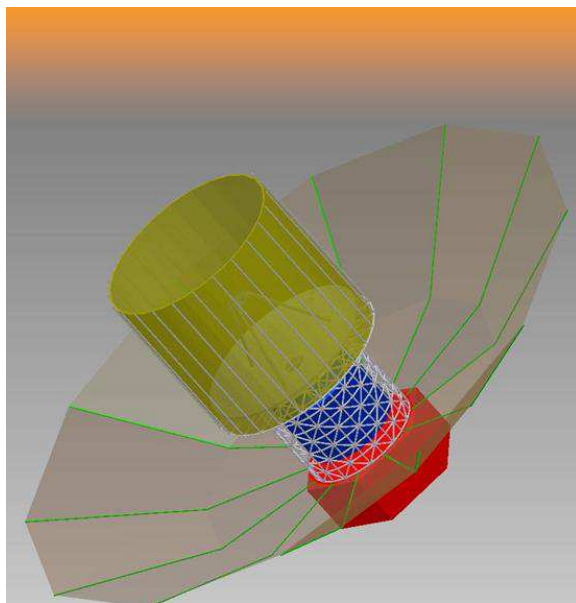


Fig. 5. Artist's impression of the SAGACE satellite. The 3-m telescope is visible through the inner shield, feeding the large cryostat (blue) cooling the spectrometer and the detector arrays. The service module is shown in red. The large deployable Sun/Earth shield is 12 m in diameter.

For our telescope and spectrometer system, photon noise limited bolometers in our bands reach NEFDs of 70, 52, 63, and 45  $\text{mJy}\sqrt{\text{s}}$  for each 20-GHz spectral bin in low-resolution mode, and 1.4, 1.0, 1.3, and 0.9  $\text{Jy}\sqrt{\text{s}}$  for each 1-GHz spectral bin



in high-resolution mode. The resulting performance in terms of the science goals is reported in Section 4.

### 3. Mission

The SAGACE satellite needs to be three-axis stabilized, with a pointing accuracy of 2 arcmin and a pointing knowledge of 15 arcsec, with a stability of 1 arcsec/s and an agility of  $90^\circ$  in 15 minutes.

The orbit of the SAGACE mission results from a cost/performance trade-off. We want to avoid ground spillover as much as possible. The best solution in this respect would be an  $L_2$  orbit similar to the Planck and Herschel orbits. We have, however, investigated cheaper solutions, including Earth Sun-synchronous orbits, medium circular orbits and elliptical orbits. The orbits have been compared assuming that

- the telescope axis has to point at more than  $135^\circ$  from the Sun and more than  $90^\circ$  from the Earth's surface throughout the mission;
- we want to reduce the spurious ground-diffraction signals below  $1 \mu\text{K}$  during observations;
- we want a duty-cycle (observation time/total time) larger than 50%;
- we do not want to spend a significant fraction of time in the inner radiation belt;
- we do not want to have a propulsion system on board; and
- we want to use only reaction wheels for the attitude control system and magnetic torquers as momentum-damping elements.

The best trade-off we have found satisfying all these requirements is a 6-hour low elliptical orbit, with 2364 km perigee and 18330 km apogee. The top three hours of the orbit are used for science observation. During the other half-orbit the telescope will point in the “safe” direction orthogonal to the orbit plane and the magnetic torquers will perform their momentum damping activity, allowing the speed of the flywheels to be maintained far from saturation. The inclination of the orbit is  $63.4^\circ$  (Molniya) to avoid the precession of the orbital plane. With a southern-hemisphere apogee, we can use just one ground station (the ASI-operated Malindi equatorial station) to control the satellite and download the data. On average this gives a contact time of 3.6 hours per day, split in four passes over the station, at satellite altitudes between 4000 and 13000 km. For the low resolution mode this is more than enough to download all the data gathered by the instrument during the 12 hours per day of observation. High resolution observations will alternate with low-resolution observations to allow the download of high resolution data stored on board.

The main disadvantage of this orbit is that it passes through the inner radiation belt, while the apogee is located inside the outer radiation belt. To mitigate the first problem, we implement rad-hard technologies for the satellite and we switch several subsystems off during the inner belt crossing. With respect to the second problem, we have carried out detailed simulations of the effect of cosmic rays on the

bolometers in the outer radiation belt. The simulation used GEANT-4 to compute the showers and assumed a slab model where each bolometer is sandwiched between two 3-mm layers of copper and two 10-mm layers of aluminium. To simulate the radiation environment along the orbit we have considered galactic cosmic rays (0.1-10 GeV), trapped electrons (0.5-6.5 MeV) and trapped protons (20-50 MeV). We find that the main contribution comes from galactic cosmic rays in the GeV range, resulting in a rate of about  $1 \text{ cm}^{-2} \text{ s}^{-1}$ . The small cross-section of spider-web bolometers then results in an acceptable rate of glitches in the data.

The total dose absorbed by electronic components inside a 10mm thickness equivalent aluminum box has been simulated using ESA's SPENVIS SHIELD-OLSE2 code, and is of the order of 10 krad in the two-year mission.

#### 4. Observation Plan and Expected Performance

The SAGACE mission has been optimized for efficient conduct of the investigations described in Section 1 in its two-year lifetime, which is set by the cryogenic hold time. In particular, 18 months of the mission will be devoted to a low-resolution ( $R = 20$  at 300 GHz) survey of the sky, with 6 months on well-known clusters and 12 months surveying blank sky regions, to discover new clusters and to produce an important AGN catalogue, and a survey of starforming galaxies over a broad redshift range with an unprecedented combination of depth and area.

The SAGACE instrument configuration will allow us to study thousands of clusters in detail (see Fig. 6) with full spectroscopic coverage in 100-450 GHz.

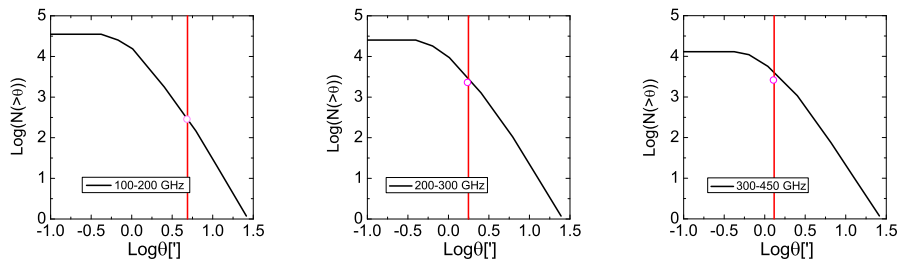


Fig. 6. All-sky cluster counts vs. intrinsic angular FWHM in the SAGACE bands 100-200 GHz (left), 200-300 GHz (middle), and 300-450 GHz, (right). A limiting flux density (per resolution element) of 20 mJy has been assumed. The angular resolution of a telescope with a 3-m primary mirror is marked by the vertical lines. Magenta dots show the expected cluster counts taking into account the confusion from radio and sub-mm unresolved sources.

In Table 1 we report sample results from a detailed Monte Carlo simulation of the recovery of parameters from SZE observations of two clusters: a large nearby cluster (A1656, with  $z = 0.0230$ ,  $\theta_c = 10.5'$ ) and a small, distant cluster (A0383, with  $z = 0.187$ ,  $\theta_c = 0.39'$ ). We have compared a ground-based three-band (95, 150, 225 GHz) photometric measurement with characteristics as in,<sup>16</sup> the Planck survey

using six bands for SZ detection and the other three for foreground removal, and the SAGACE survey. The higher resolution and longer integration time (with respect to Planck) and the wide continuous spectral coverage of SAGACE lead to far superior results. Not only are the errors greatly reduced (by a factor 6-7 with respect to Planck for small clusters), but also distributions of the recovered parameters are much less skewed, implying a lower bias in their estimates.

Table 1. Parameters Estimation Comparison

Cluster	Parameter	input value	SPT	Planck	SAGACE
A1656	$v_p$ (km/s)	0	$210 \pm 450$	$37 \pm 79$	$-31 \pm 32$
A1656	$\tau$	0.00859	$0.009 \pm 0.001$	$0.0088 \pm 0.0002$	$0.0085 \pm 0.0002$
A0383	$v_p$ (km/s)	0	$10 \pm 530$	$-410 \pm 910$	$-20 \pm 140$
A0383	$\tau$	0.01924	$0.025 \pm 0.007$	$0.0127 \pm 0.0077$	$0.0186 \pm 0.0011$

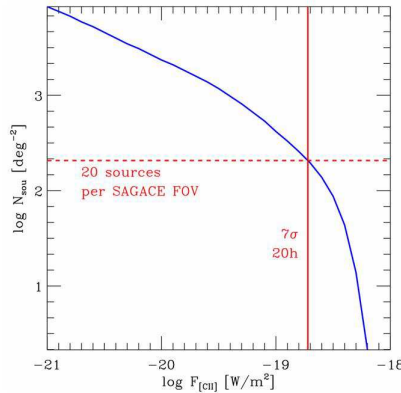


Fig. 7. Cumulative counts of galaxies with [CII] line flux above a given level in the 720-760 GHz band (the highest frequency band of SAGACE) predicted by the model in.<sup>15</sup> The red line shows the expected  $7\sigma$  detection limit at high resolution ( $R = 740$ ) with an integration time of 20 hours. With such an integration we can sample the knee of the counts, i.e., maximize the number of detected sources and sample those galaxies dominating the line emission at  $z \sim 1.5$ .

The remaining six months of the mission will be devoted to a high-resolution ( $R = 700$  at 700 GHz) survey whose main output will be a catalog of galaxies in the redshift desert detected in the [CII] line. In Fig. 7 we show how many galaxies it is possible to detect in this way.

## 5. Conclusions

We have studied the implementation of a spectroscopic survey of the mm/sub-mm sky on a small (cost-wise) space mission. Taking advantage of the differential design

of the spectrometer, we have shown that a sensitive mission can use an elliptical Earth orbit, reducing the cost of the launcher and of the attitude control system. The two blind surveys to be performed by SAGACE, and the extensive plan of pointed observations of galaxy clusters, will provide a unique database for cosmological and astrophysical studies of cosmic structures. Such a database will have a number of applications for cosmology, high-energy astrophysics and astro-particle physics.

### Acknowledgements

The phase-A study of SAGACE has been supported by the Italian Space Agency (ASI) and by the Balzan Foundation.

### References

1. Lamarre J. M., et al., *New Astron. Reviews*, 47, 1017-1024, (2003)
2. Lawrence C. R., et al., *New Astron. Reviews*, 47, 1025-1032 (2003)
3. Fixsen D.J., et al., *Astrophys.J.* 473 , 576, (1996)
4. Griffin M., et al. *Space Telescopes and Instrumentation I: Optical, Infrared, and Millimeter*, Proceedings of the SPIE, 6265, 62650A, (2006).
5. Yun et al., *Astrophys.J.* 528, 171 (2000)
6. Colafrancesco S., *NewAR*, 51, 394C, (2007)
7. Renzini A., & Daddi E., *Msngr* 137, 41 (2009)
8. Luhman K.L., et al. , *ApJ*, 594, 758 (2003)
9. Maiolino R., et al. *A&A*, 440, L51, (2005)
10. Maiolino R., et al. *A&A*, 500, L1, (2009)
11. Iono D., et al., *ApJ*, 645, L97, (2006)
12. Martin D., & Puplett E., *Infrared Physics* 10, 105109, (1970).
13. Burkert P., Fergg F., & Fischer H., *IEEE Trans. Geosci. Remote Sensing GE-21*, 345 (1983).
14. Carli B., Mencaraglia F., *Int. J. IR and mm waves*, 2, 1045-1051, (1981)
15. Lapi A., et al., *ApJ*, 650, 42-56 (2006)
16. Staniszewski, Z., et al., *ApJ*, 701, 32-41 (2009)